 doi:10.20944/preprints202105.0705.v1

Article

Post-fire susceptibility to brittle fracture of selected steel grades used in construction industry – assessment based on the instrumented impact test

Mariusz Maslak [1]*,Michal Pazdanowski [2], Marek Stankiewicz[3] and Paulina Zajdel [4]

[1] Cracow University of Technology, Cracow, Poland; mmaslak@pk.edu.pl
[2] Cracow University of Technology, Cracow, Poland; michal@l5.pk.edu.pl
[3] Cracow University of Technology, Cracow, Poland; goziolko@cyfronet.pl
[4] Cracow University of Technology, Cracow, Poland; paulinazajdel22@gmail.com
* Correspondence: mmaslak@pk.edu.pl; Tel.: 48501546577

Abstract: The change in the value of the breaking energy is discussed here for selected steel grades used in building structures after subjecting the samples made of them to episodes of heating in the steady-state heating regime and then cooling in a simulated fire conditions. These changes were recorded based on the instrumented Charpy impact tests, in relation to the material initial state. The S355J2+N, 1H18N9T steels and also X2CrNiMoN22-5-3 duplex steel were selected for detailed analysis. The fire conditions were modelled experimentally by heating the samples and then keeping them for a specified time at a constant temperature of: 600°C (first series) and 800°C (second series), respectively. Two alternative cooling variants were investigated in the experiment: slow cooling of the samples in the furnace, simulating the natural fire progress, without any external extinguishing action, and cooling them in water mist simulating an extinguishing action by a fire brigade. The temperature of the tested samples was set at the level -20°C and alternatively at the level + 20°C. The conducted analysis is aimed at assessing the risk of sudden, catastrophic fracture of load-bearing structure made of steel degraded as a result of a fire previously occurred with different development scenarios.

Keywords: fire; structural steel; steady-state heating regime; impact test; breaking energy.

1. Introduction

The suitability assessment of structural steel used in construction industry for possible further use after fire will be reliable only if, in the prepared expert opinion following the fire, the conventional inventory of permanent displacements and deformations found on site [1] is enriched with at least a set of appropriately interpreted results of experimental tests on basic material properties. In traditional approach those experiments are usually limited to the analysis of changes in the yield limit and modulus of elasticity of the considered material, registered after cooling and related to the initial values of those parameters before the fire exposure. In this paper we intend to draw the reader's attention to the fact that so narrowly focused research program is insufficient and in addition lacks sufficient reliability. The steel, after undergoing several episodes of monotonous but often chaotic heating, then annealing in high and usually close to constant temperature, followed by cooling down, slow if occurring by natural convection in fresh air, or rapid and sudden if induced by fire extinguishing action, although seemingly still the same is only apparently the same. In such situation it is a material structurally different from the initial material, and this means, that both its strength properties and functional values may significantly differ from those expected and forecast for the future by the expert conducting the assessment. The temperature of steel during fire episodes acting on it is often close to the temperature programmed and applied during manufacturing process to anneal and

Preprints (www.preprints.org) | NOT PEER-REVIEWED | Posted: 28 May 2021 doi:10.20944/preprints202105.0705.v1

normalize its properties, and thus is capable of initiating various changes in its microstructure, in particular grain size growth and shape changes, chaotic grain reordering resulting in loss of advantageous banded structure developed during manufacturing process [2], graphitisation and spheroidization of grains [3], and most importantly creation of additional secondary precipitates [4]. Due to the random character of the thermal action induced by a fire, inconsistent with the scenario especially designed for the given steel grade in metallurgical processes, these changes are usually of detrimental character, weakening consistency of the structure [5], and in addition are permanent as being associated with the accumulation of gradually occurring local damage. Thus the steel cooled after fire may, usually without exhibiting any changes visually observable during traditional assessment conducted in order to evaluate its suitability for prolonged use, irrecoverably loose its plastic properties and thus turn into material prone to initiation and following unrestricted propagation of brittle fracture. This type of threat is very dangerous to the potential user of structure made of such steel, as it may result in sudden and unexpected failure, initiated without exhibiting any signs preceding the incident. Therefore it is postulated to add the test of real susceptibility to brittle fracture, as a recommended test, to the set of basic tests conditioning rational conclusions regarding the possibility of further application of structural steel cooled after undergoing a fire incident in building structures [6]. In our opinion the instrumented Charpy impact test [7-11] should be recommended in this field. In the following part of this paper we will show the way of interpreting the results obtained after application of this test [12,13]. We will also refer to the detailed results of experimental research conducted by us on selected steel grades commonly used in contemporary construction industry [14].

2. Interpreting of impact notch-toughness test results in terms of assessing the steel susceptibility to brittle failure

The $F-s$ curve depicting the dependency between breaking force $F\ \left[\mathrm{kN}\right]$ and displacement $s\ \left[\mathrm{mm}\right]$ registered at the force application point is the basic result obtained for a steel sample subjected to a instrumented impact notch-toughness test. This curve is unequivocally related to the relationship between the breaking work $KV=W_t\ \left[\mathrm{J}\right]$ (usually interpreted as the energy dispersed during breaking of the sample) and the same displacement. The energy is quantified by the area bounded by the $F-s$ curve, thus the following holds:

$$W_t=\int_{s=0}^{s_i}F\left(s\right)ds \tag{1}$$

Based on those curves conclusions are drawn regarding the susceptibility of given material to the initiation of brittle fractures. The conditions for potential propagation of such fractures are also forecast, i.e. whether the propagation will be stable and to what degree will be susceptible to self-arrest [15]. The samples after notch-toughness test may exhibit a fully plastic, completely brittle, or possibly in the most general case a mixed breakthrough [16]. In Figure 1 a typical theoretical $F-s$ curve is depicted, usually obtained for a mixed breakthrough. The characteristic points indicating bounds for the subsequent phases of crack development are indicated there as well (according to the standard [17]).

The force F_{gy} on this graph is usually associated with plastic initiation of developing breakthrough, while the force F_m located at the apex of the $F-s$ curve indicates, together with the accompanying displacement, the end of the stable fracture initiation phase. With further increasing displacement the already initiated fracture undergoes stable development phase, such that its propagation is accompanied by plastic deformation. The initiation of unstable fracture growth phase occurs only when the displacement associated with force F_{iu} is reached. This phase is ended when the displacement associated

Preprints (www.preprints.org) | NOT PEER-REVIEWED | Posted: 28 May 2021 doi:10.20944/preprints202105.0705.v1

with force F_a is arrived at. At this moment the effective self-arresting of the fracture, so far progressing in an unstable manner, is initiated and as a consequence the specimen transits into the phase of plastic breaking [18].

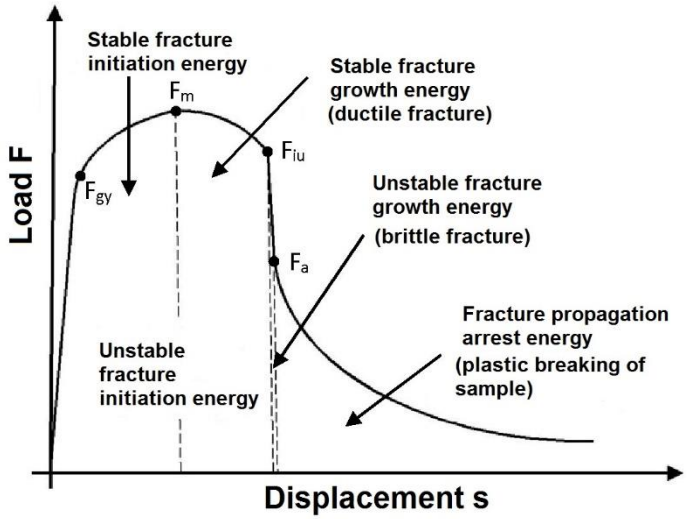

Figure 1. Theoretical $F-s$ curve obtained during impact notch-toughness test of steel specimens exhibiting mixed breakthrough.

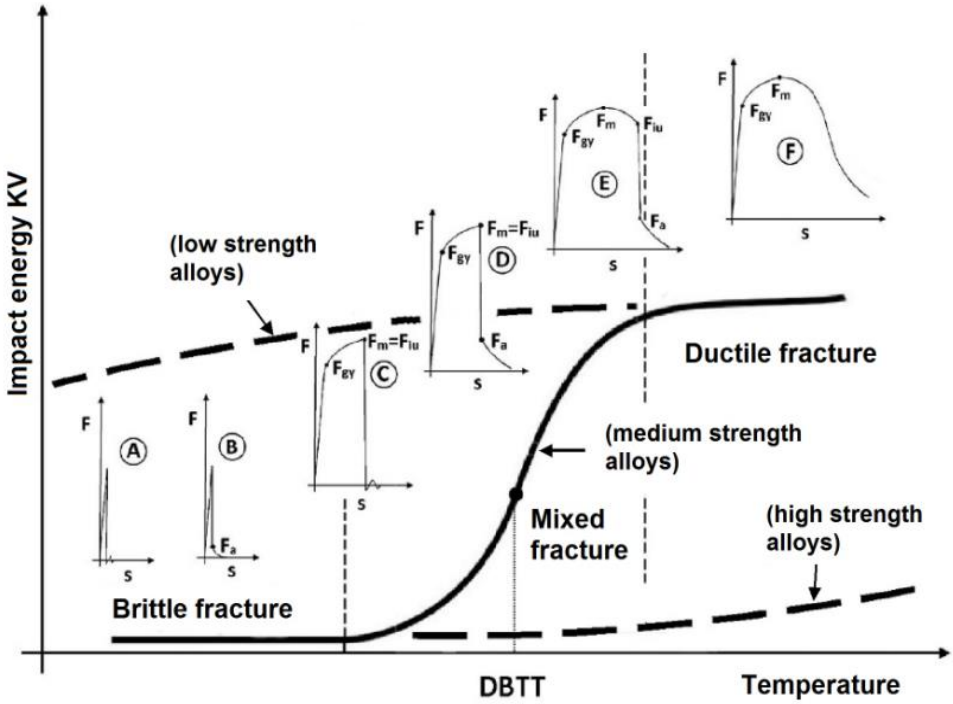

Figure 2. Location of standard $F-s$ curves on $KV-T$ graph (description in the text)

According to the code [19] the shape of the $F-s$ curve obtained during experiment should be associated with one of the standard shapes, denoted by successive letters *A*, *B*, *C*, *D*, *E* and *F* (Figure 2). For the extreme shape, denoted by symbol *A*, only unstable, i.e. brittle fracture growth occurs during the whole process. The second extreme shape in this set is denoted by letter *F*. The process conforming to this shape does not exhibit unstable fracture growth at any moment. All breakthrough development phases are stable then, and this means that self-arresting of the fracture is fully effective. The larger the area

Preprints (www.preprints.org) | NOT PEER-REVIEWED | Posted: 28 May 2021 doi:10.20944/preprints202105.0705.v1

under the $F-s$ curve obtained during the test, however, determined for the displacement greater than that associated with the limiting force F_a, the greater the capability of the sample material to efficiently arrest the unstable growth of previously initiated fracture. This in turn results in an appropriately larger area of ductile breakthrough observed on the fracture [20].

The code shapes of the $F-s$ curves are assigned to particular locations, this time depicted on the graph exhibiting relationship between the specimen breaking energy ($KV\left[\mathrm{J}\right]$) and the testing temperature ($T\ \left[^{\circ}\mathrm{C}\right]$). Inference on steel brittleness is related here to the limiting value of the breaking energy $KV_{\min}=27\left[\mathrm{J}\right]$ associated with ductile to brittle transition temperature (*DBTT*) [21]. The steels, for which in given testing temperature a breaking energy lower than $KV_{\min}$ has been experimentally obtained (i.e. those conforming to the shapes *A*, *B*, *C* and *D*) in general exhibit dominating brittle character of fracture, and as such do not exhibit the capability to effectively self-arrest initiated brittle fractures, and therefore are not recommended for application in construction. The steels exhibiting such capability (i.e. only those conforming to the shapes *E* and *F*) are characterized by the $F-s$ curves located to the right of the threshold *DBTT* temperature [22].

3. Brittle fracture development zones and their structural conditioning

The typical breakthrough of a steel sample obtained during impact notch-toughness test for a mixed breakthrough is depicted in Figure 3c. As shown, the fracture is initiated directly under the notch, though the pendulum strikes on the other side of the specimen (Figure 3b). This is due to the local concentration of stresses under the notch (Figure 3a).

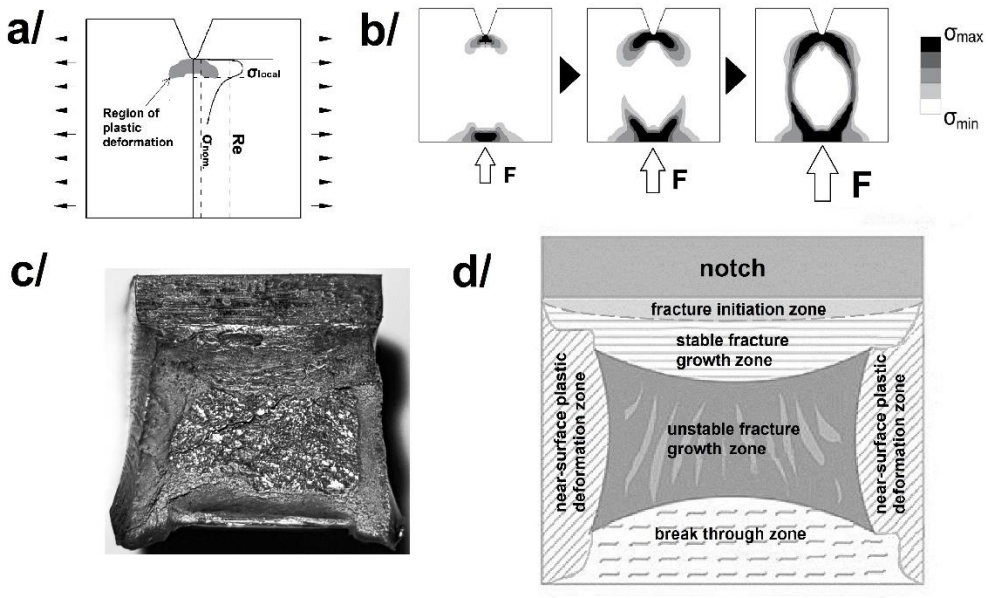

Figure 3. Notch effect on an ISO Charpy V steel sample: a) local concentration of stresses under the notch crest as a result of pendulum strike, b) numerical simulation of stress field development in a broken specimen, c) typical breakthrough of mixed character, d) identification of zones on the mixed breakthrough.

The following fracture development phases may be observed on the fracture surface. The surfaces of all regions denoted in Figure 3d correspond in percent to the phases of this process, as registered on $F-s$ curve (Figure 1). As the number of degrees of freedom on the sides of the specimen is larger than on the inside, in these zones ductile fracture may occur. Unstable brittle fracture dominates the picture on the inside part of the specimen.

 doi:10.20944/preprints202105.0705.v1

Brittle and plastic breakthroughs should be associated with qualitatively different fracture mechanisms. On one hand inclusions such as for instance carbides, oxides, borides, nitrides or silicates are incoherent with the crystallographic matrix and thus constitute a crystalline void. Their presence induces the fracture mechanism dominated by brittle fracture. On the other hand presence of manganese sulfites in the steel structure may lead to domination of plastic fracture. The difference in action of both inclusion groups indicated above is that the thermal expansion coefficients of inclusions belonging to the first group are lower than the analogous coefficients of the crystallographic matrix, thus the crystallographic matrix „tightens" over an inclusion in a sense. In the case of manganese sulfites the value of corresponding thermal expansion coefficient is higher than the value of analogous coefficients for crystallographic matrix, thus the inclusion tightens itself within the matrix and a „void" is developed. The oxides and silicates (and the remaining inclusions belonging to this group) represent good brittle fracture initiators, as continuity between dislocation network in the crystallographic matrix and brittle particle is assured, while manganese sulfites in such approach represent initiators of voids leading to initiation of ductile fracture [23,24]. Brittle fracture observed on test samples cooled after prior exposure to fire temperature may also be explained as a consequence of unwanted so called sigma phase separation in their structure (this pertains only to certain acid resistant steels of grade 18/10). In the theoretical description the brittle fracture process in carbon and low alloy steels usually comprises three stages, in the following sequence: crack nucleation on particles (of for instance carbides), propagation of these cracks on phase boundaries between carbides and ferrite, and finally propagation of the fracture on the first ferrite-ferrite grain boundary [25].

4. Description of the impact notch-toughness test conducted

The purpose of the experimental research conducted by us may be stated as verification of the suitability for use of selected steel grades commonly used in construction industry after undergoing a fire event. We intend to verify, whether the samples made of these steel grades, cooled after preceding exposure to fire temperature, will prove prone to brittle fracture, as this would disqualify these steels from potential further service, especially under load. The following steel grades have been selected for the detailed investigation:

- **S355J2+N** steel – low alloy two phase ferritic-pearlitic with stranded perlite, raised manganese content, subjected to normalization, representing a group of steels exhibiting low sensitivity to short time thermal action (in the temperature below 350ºC),
- **1H18N9T** steel – Cr-Ni high alloy, single phase, acid resistant, austenitic with carbon stabilized by the addition of titanium, supersaturated with a temperature of approximately 1100ºC, representing a group of steels recommended for use at the temperature values not exceeding 600ºC (due to the risk of unwanted sigma phase separation at the temperature range of 650ºC – 850ºC),
- **X2CrNiMoN22-5-3** steel – high alloy, two phase, austenitic-pearlitic, of the duplex type, supersaturated with a temperature of approximately 1050ºC in water, representing a group of duplex steels recommended for use at the temperature values not exceeding 300ºC (due to the occurrence of unfavourable 475ºC brittle failure phenomenon).

As indicated above, these steels are considered to be representative for the whole groups of steel grades applied in construction with respect to experimental results expected by us.

Preprints (www.preprints.org) | NOT PEER-REVIEWED | Posted: 28 May 2021 doi:10.20944/preprints202105.0705.v1

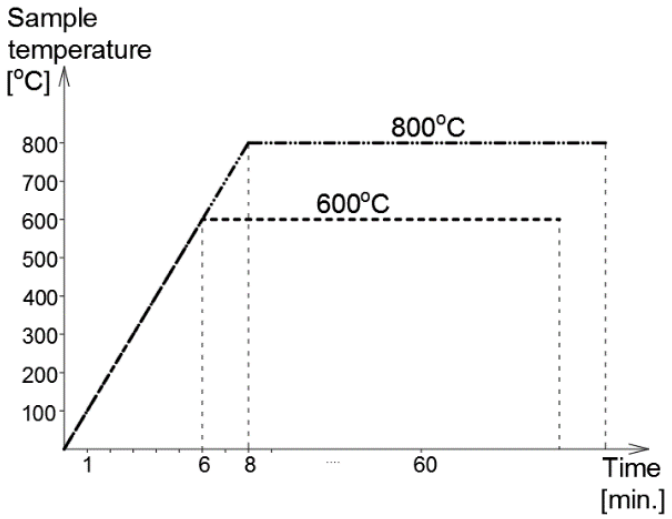

Figure 4. Fire action simulated during research.

In our research the susceptibility of steel to brittle fracture after surviving a fire incident has been verified on an instrumented Charpy impact notch-toughness test [26], with the physical action of fully developed fire simulated by a proper preparation of test samples [14]. Prior to the test these samples have been subjected to thermal action of formalized course. During the first phase of this process these samples had been heated to the temperature of 600ºC (first set) or 800ºC (second set), respectively, then kept for 60 minutes at this constant raised temperature, conforming to the conventional steady state heating regime (Figure 4). Following the conclusion of the heating the samples have been cooled to the room temperature. During the tests, for comparative purposes, two alternative cooling scenarios have been applied, namely slow cooling of samples in the furnace, simulating self-extinguishing of fire, and cooling in the water mist corresponding to the intervention of fire brigade.

The impact notch-toughness tests of samples prepared in advance have been conducted conforming to the recommendations of the EN ISO 14556 code on an instrumented Charpy pendulum JB-W450E-L (Figure 5), having the potential energy of 450 J. The R8 (American type) pendulum hammer has been selected for the tests, as it is understood that in construction industry an impact by a flat surfaced object is more probable (with respect to the classical R2 pendulum hammer of European type) [27]. The hammer was equipped with a transducer used to measure the force hitting the specimen, and the displacement of the force application point accompanying the load application sequence was measured with an encoder. The signals delivered by both transducers were collected and processed by a data logger of high sampling frequency and finally analyzed by specialized software designed for that purpose. The results of each test were recorded and depicted on automatically generated graphs displaying the force, energy and displacement as functions of time or force and energy as functions of displacement. The software automatically indicated on those graphs the locations of characteristic limit points as well.

The destructive tests have been conducted in the temperature of +20ºC (simulating summer conditions) and alternatively in the temperature of –20ºC (to simulate winter conditions). Each time the $F-s$ curve (Figure 1) and the corresponding W_t-s graph have been recorded. In addition the longitudinal expansion *LE* [mm] of broken samples has been measured as well (Figure 6).

Preprints (www.preprints.org) | NOT PEER-REVIEWED | Posted: 28 May 2021 doi:10.20944/preprints202105.0705.v1

Figure 5. Instrumented Charpy pendulum used to conduct the tests.

Figure 6. Measurement device used to measure the longitudinal expansion *LE*.

Performed tests included 30 qualitatively different measurement cases. For each of the considered steel grades and each of two temperature values four independent test cases related to steel after initial heat treatment (two heating regimens times two cooling scenarios) and one case related to the untreated steel in the virgin state (without initial heat treatment) have been conducted. Each measurement case consisted of test performed on six independent steel samples, to assure sufficient reliability of the final estimate obtained. Final test results for a measurement case have been averaged over these six samples. Thus over all $30 \cdot 6 = 180$ independent impact notch-toughness tests have been conducted.

Reduction of the data sets obtained during the experiment to $F - s$ and $W_t - s$ graphs averaged for each measurement case, and averaged value of the longitudinal expansion *LE* allowed for simplified treatment in the analysis of the random variability in the impact toughness sought. The final results have been archived, using three digit notation scheme applied to separate test cases, with consecutive digits interpreted as shown in Table 1. The case denoted with single digit 1, 2 or 3 in this notation denotes the set consisting of six individual tests performed on steel remaining in the initial virgin state (a sample which did not undergo the preliminary heat treatment).

Table 1. Description mode of the samples subjected to impact testing

Preprints (www.preprints.org) | NOT PEER-REVIEWED | Posted: 28 May 2021 doi:10.20944/preprints202105.0705.v1

First digit - steel grade	Second digit – heating temperature	Third digit – cooling mode	Test temperature
1 – S355 **2** – 1H18N9T **3** – X2CrNiMoN22-5-3	**6** – 600ºC **8** – 800ºC	**0** – cooling in the furnace **1** – cooling in water mist	+20ºC –20ºC

All the considered tests related to the S355J2+N and 1H18N9T steels have been conducted on full size ISO Charpy V-10 samples. In the analogous cases related to X2CrNiMoN22-5-3 duplex steel the samples had to be reduced in size to ISO Charpy V-7.5 [28], as the potential energy of the 450 J pendulum proved to be insufficient to break these samples both in the initial state, as well as after heating simulation conducted in the temperature of 600ºC during one hour and rapid cooling in water mist.

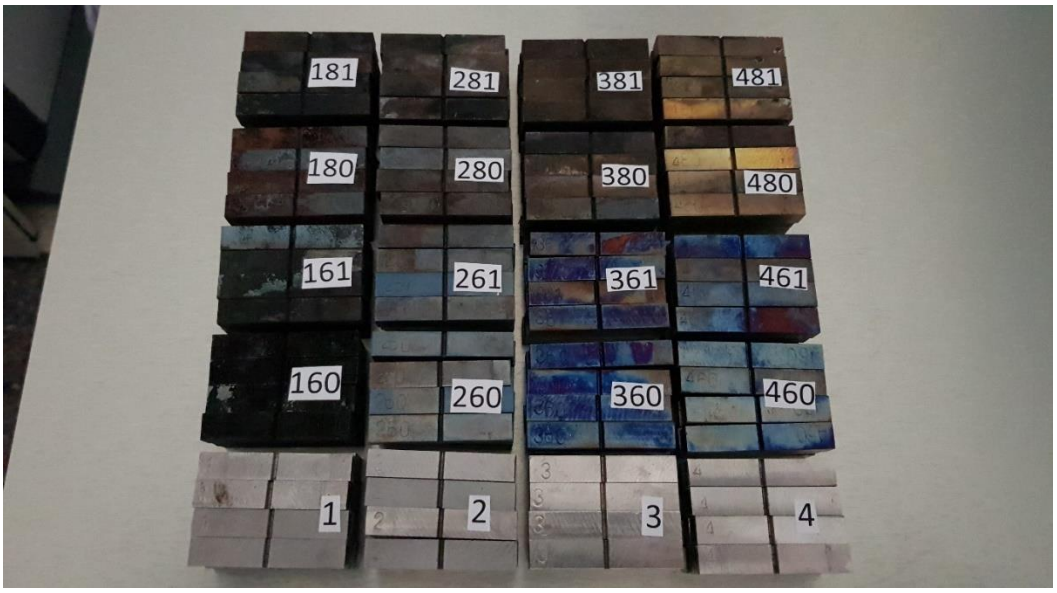

Figure 7. Samples prepared for impact notch-toughness test, made of (counting from left): S355J2+N steel (group 1), 1H13 steel (group 2), 1H18N9T steel (group 3) and X2CrNiMoN22-5-3 steel (group 4). The results obtained for 1H13 steel are not discussed here. Therefore the samples belonging to group 3 are denoted as group 2 and belonging to group 4 as group 3 in the Table 1.

The impact notch-toughness test samples made of the steel grades analyzed by us are depicted in Figure 7. These samples are coded in a coding system different from the one listed above in the Table 1, as the results obtained for the 1H13 steel have been skipped in the following analysis. Let us note the different colouring of the scale visible on the surface of individual groups of samples, induced by different chemical composition of the substrate. The scale observed on samples made of S355J2+N steel was loosely bonded to the underlying material, while on the samples made of 1H18N9T and X2CrNiMoN22-5-3 steels it formed a tight top layer.

Observation of the notch profile on the samples in the initial state, on the notch profile projector XT-50 (Figure 8), has shown, that the notches made were located just below the upper tolerance limit prescribed by the code [29]. Repeated observation of the notches after heat treatment and removal of the scale induced by steel surface oxidation revealed increase in their size, so in a few cases their size slightly exceeded the tolerance allowed. According to the provisions of the standard [30], changes of this type may result in an increase in the breaking energy by about 2÷3 J in brittle samples and by a negligible value

Preprints (www.preprints.org) | NOT PEER-REVIEWED | Posted: 28 May 2021 doi:10.20944/preprints202105.0705.v1

in ductile samples. Due to so low value of the energy, in the following considerations the systematic error of impact notch-toughness estimated, in the identified cases where the upper limit of the notch profile tolerance has been exceeded, has been disregarded.

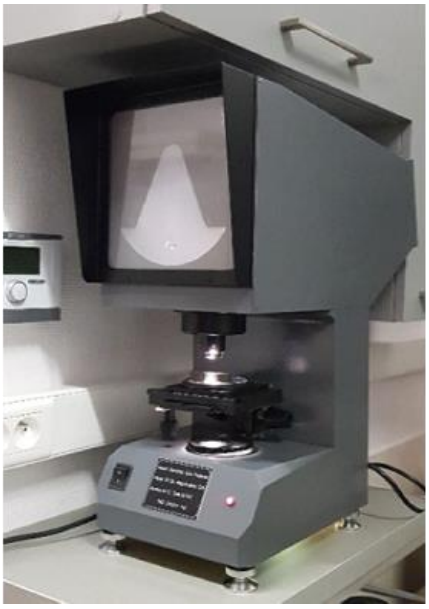

Figure 8. The notch profile projector XT-50 used during the tests to verify whether the notch size tolerance criteria have been observed.

5. Detailed analysis of the obtained results

5.1. S355J2+N steel

The averaged $F-s$ curves obtained for this steel in the temperature of +20ºC are depicted in Figure 9a, while those obtained in the temperature of –20ºC are depicted in Figure 9b, correspondingly. The first group of these results (depicted in Figure 9a) after comparison against sample curves included in the code (according to [19]) may be qualified as conforming to the *F* type curve, denoting plastic zone devoid of unstable crack growth area. The second group (depicted in Figure 9b) corresponds to the *D* type curve, unequivocally revealing the area of unstable crack growth. Let us note, however, that in this case the unstable crack growth area had only limited reach, as the material exhibited the capability of effectively arresting the brittle crack growth by plastic self-restraint.

In Figure 10 the $W_t - s$ relationships are depicted, obtained by us for S355J2+N steel and corresponding to the $F-s$ graphs shown in Figure 9 (curves depicted in Figure 10a correspond to graphs presented in Figure 9a, while analogous curves of Figure 10b correspond to graphs presented in Figure 9b). It has to be emphasized, that the considered steel in the initial state and in the testing temperature of +20ºC (Figure 10a – group of samples denoted with digit 1) exhibited higher values of the breaking energy W_t (117 J) as well as averaged longitudinal expansion *LE* (1.94 mm) when compared with the remaining samples made of the same steel, but subjected to the preliminary heat treatment. However, in the case of tests conducted in the temperature of –20ºC the opposite proved to be true. Both the averaged breaking energy W_t (26 J) and the averaged longitudinal expansion *LE* (0.56 mm) determined on samples in the initial state (Figure 10b – a group of samples denoted with digit 1) were lower than the corresponding values determined on samples subjected to the preliminary heat treatment.

Preprints (www.preprints.org) | NOT PEER-REVIEWED | Posted: 28 May 2021 doi:10.20944/preprints202105.0705.v1

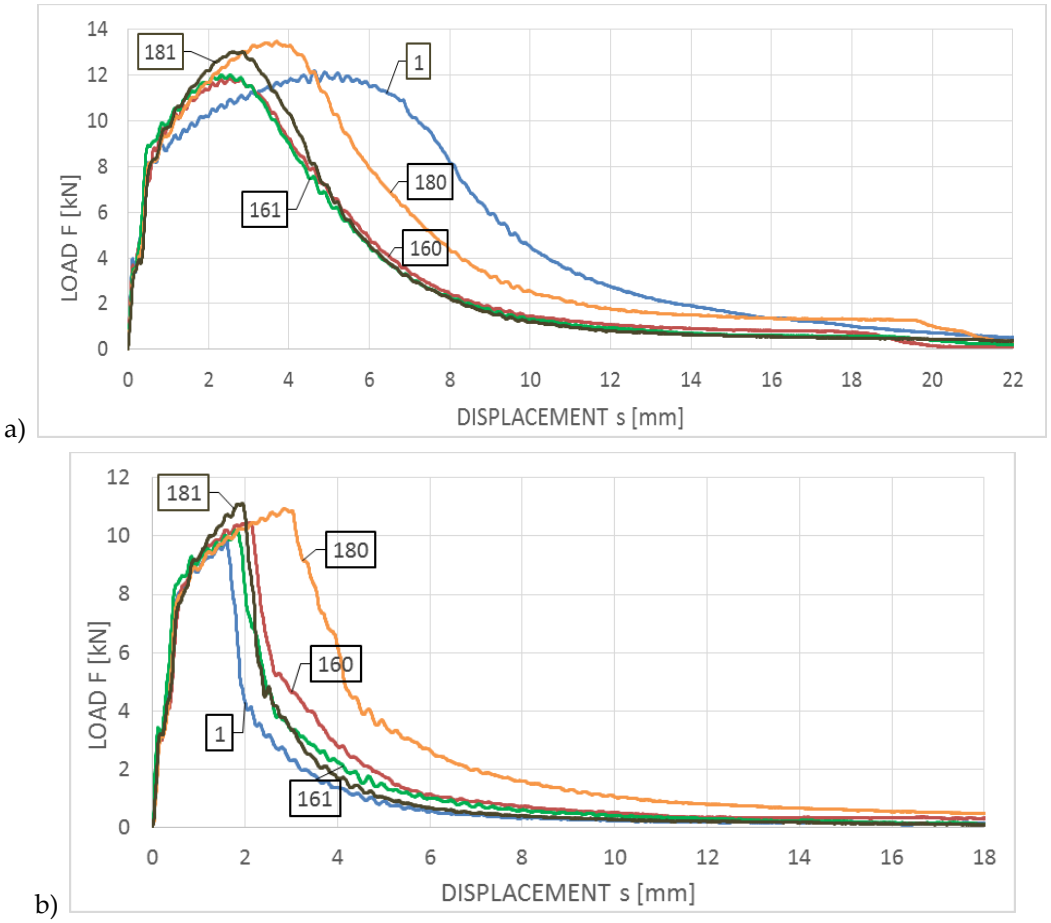

Figure 9. Averaged $F-s$ curves obtained on samples made of S355J2+N steel: a) during tests conducted in +20ºC, b) during tests conducted in -20ºC.

In addition, the cooling mode significantly affected the behaviour and properties of the samples analyzed, if only these samples have been subjected to heating in the temperature of 800ºC (with respect to the impact notch-toughness test conducted in both temperature values of +20ºC and –20ºC). Heating to so high temperature usually results in partial austenitization of the steel structure [31]. The following slow cooling of the sample in the furnace (sample marked as 180) leads under those circumstances to the development of structure containing spheroidal carbides uniformly distributed in the ferritic lattice, and this results in increased plasticity and impact strength. Fast cooling with water (sample 181) has its consequences in carbon oversaturation of a part of ferrite formed from austenite and hardening of steel, and thus decreased plasticity and impact strength. This phenomenon has not been observed on samples heated to 600ºC only. The shapes of curves associated with samples 160 and 161 were very similar, as can be observed on both Figure 10a and Figure 10b. For the reasons listed above the results obtained for the specimens denoted with 180, regardless of the temperature at which the impact test has been made, definitely stood out from all other simulations conducted for this steel. The remaining scenarios, both those associated with the heating temperature of 600ºC (regardless of the cooling mode), and the heating temperature of 800ºC followed by cooling with water yielded similar results expressed by similar shape of the $F-s$ curves and thus estimated values of the breaking work W_t (60÷74 J for the tests conducted at +20ºC and 31÷35 J for the tests conducted at –20ºC, respectively) and longitudinal extension *LE* (1.05÷1.37 mm for the tests conducted at +20ºC and 0.73÷0.89 mm for the tests conducted at –20ºC, respectively).

Preprints (www.preprints.org) | NOT PEER-REVIEWED | Posted: 28 May 2021 doi:10.20944/preprints202105.0705.v1

a)

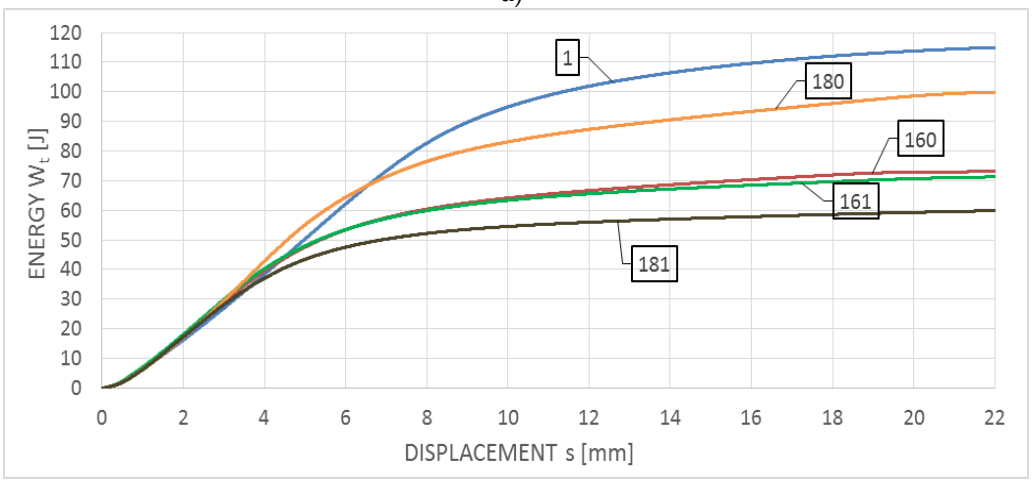

b)

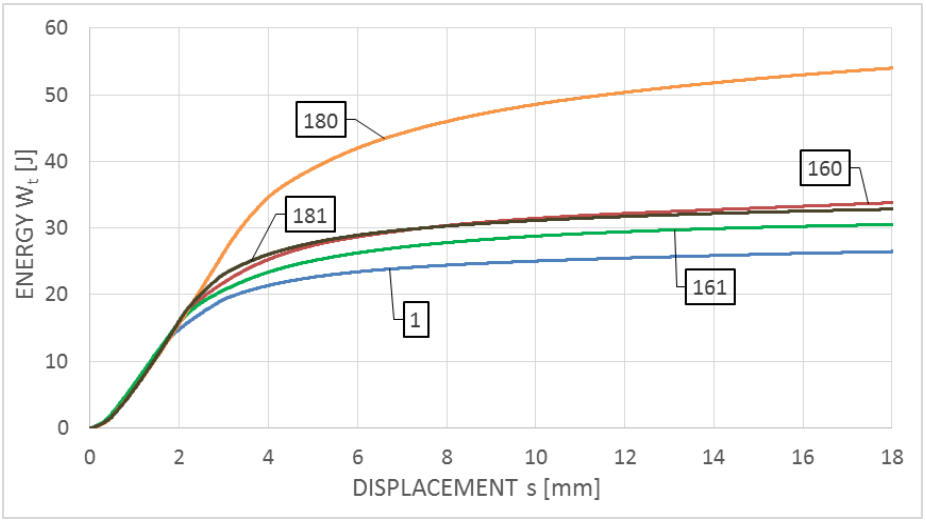

Figure 10. Averaged $W_t - s$ curves obtained on samples made of S355J2+N steel: a) during tests conducted in +20ºC, b) during tests conducted in –20ºC.

5.2. 1H18N9T steel

Averaged $F - s$ curves obtained for this steel are depicted in Figure 11a with respect to the impact strength tests conducted in the temperature of +20ºC, and Figure 11b – with respect to the analogous tests conducted in the temperature of –20ºC. The corresponding $W_t - s$ graphs are juxtaposed on Figure 12a and Figure 12b. The curves depicted on both figures this time correspond to the *F* type curves, with plastic zone devoid of unstable crack growth area. All the samples made of this steel regardless of the testing temperature are characterized by a fully plastic fracture (though, of course, the steel tested in the temperature of +20ºC proved to exhibit higher plastic properties than the one tested in the temperature of –20ºC). The breaking work W_t value obtained during the tests conducted in +20ºC remained within the span of 251÷330 J, while the same work obtained during tests conducted in –20ºC remained within the span of 171÷240 J. The obtained values of longitudinal extension *LE* remained within 1.51÷1.94 mm (obtained at the temperature of +20ºC) and 1.77÷2.00 mm (obtained at the temperature of –20ºC).

Preprints (www.preprints.org) | NOT PEER-REVIEWED | Posted: 28 May 2021 doi:10.20944/preprints202105.0705.v1

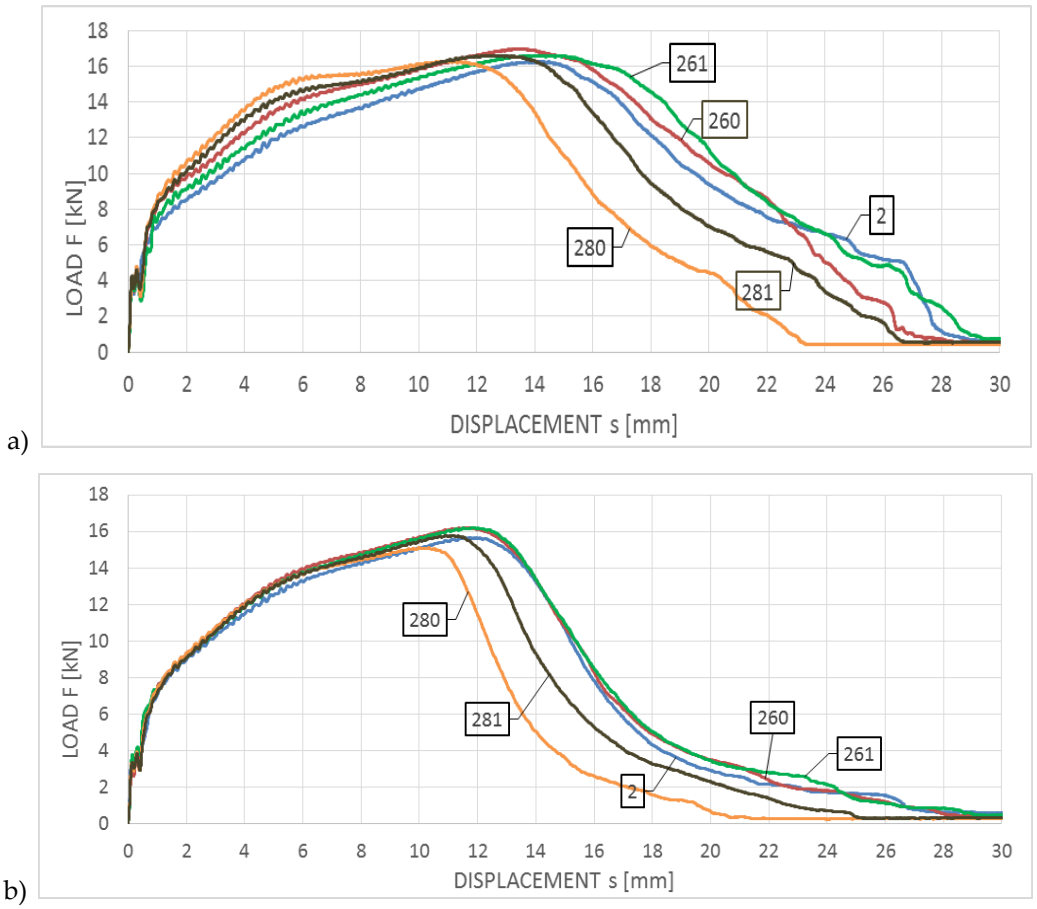

Figure 11. Averaged $F-s$ curves obtained on samples made of 1H18N9T steel: a) during tests conducted in +20ºC, b) during tests conducted in –20ºC.

The largest decrease in the breaking work with respect to the untreated material has been observed for this specimen (the group of tests denoted with digit 2) in heating scenarios assuming heating up to 800ºC. This temperature is located in the upper limit of the harmful σ phase precipitation range in the 18/9 class austenitic steels. Slow cooling from this level (the group of tests denoted with number 280) results in a relatively long transfer time of this steel through the zone associated with precipitation of the harmful phase. Fast cooling with water mist (the group of tests denoted with number 281) results in freezing of the microstructure with lower content of the phase σ, and thus lower reduction of the breaking work. Heating of the tested steel in the temperature of 600ºC does not result in the precipitation of this type, thus in such case reduction of the averaged breaking work measured in the toughness test of samples subjected to simulated fire action, as compared to the samples made of the material unaffected by simulated fire, did not occur (and even certain increase has been observed), regardless of the temperature at which the tests have been conducted.

5.3. X2CrNiMoN22-5-3 steel

The averaged impact strength tests authoritative for this steel are juxtaposed in Figure 13a with respect to the tests conducted in +20ºC, and Figure 13b with respect to the tests conducted in –20ºC. The $W_t - s$ relationships corresponding to these tests are depicted in Figure 14a and Figure 14b, respectively.

Preprints (www.preprints.org) | NOT PEER-REVIEWED | Posted: 28 May 2021 doi:10.20944/preprints202105.0705.v1

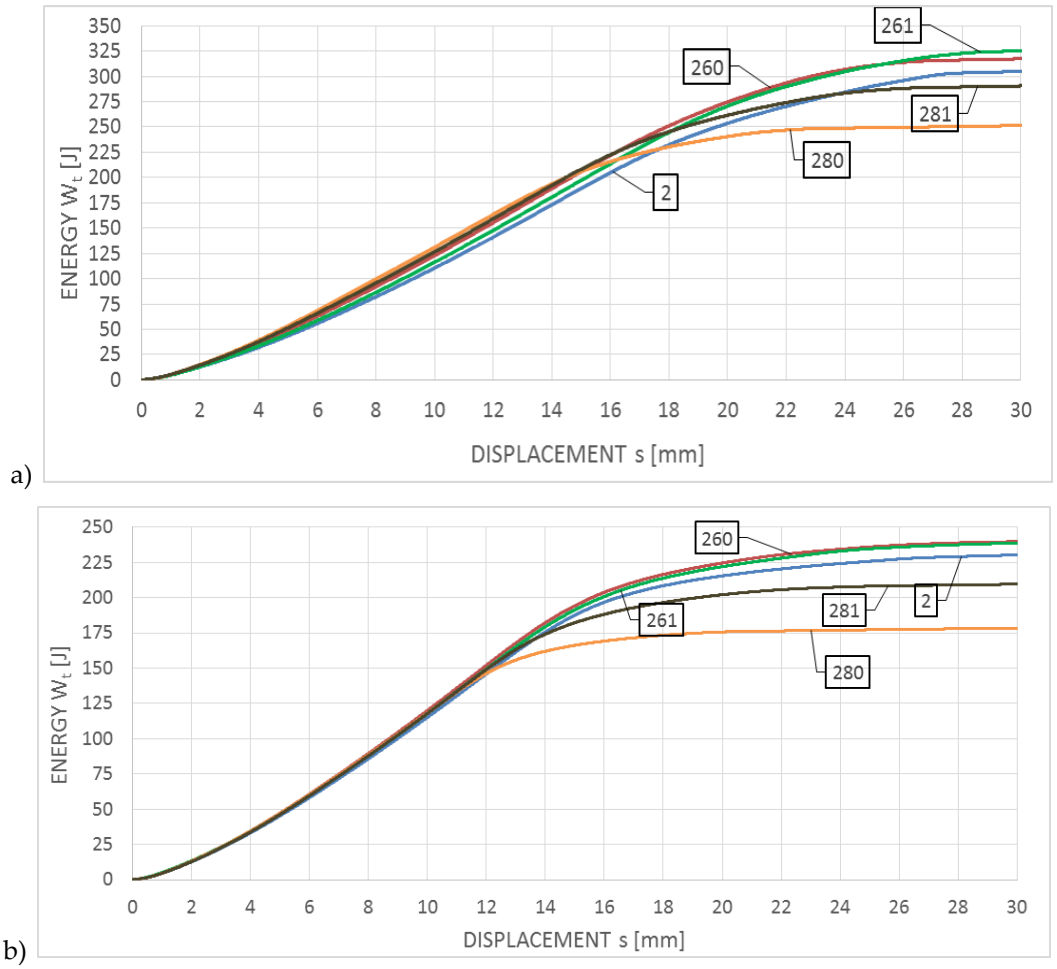

Figure 12. Averaged $W_t - s$ curves obtained on samples made of 1H18N9T steel: a) during tests conducted in +20ºC, b) during tests conducted in –20ºC.

As may be observed on these graphs, all the curve sets depicted may be assigned to the group *F*, in spite of substantial differences observed in the breaking work W_t obtained for particular scenarios of the simulated fire. All the curves are devoid of unstable crack growth zone. For the samples made of steel remaining in the initial state (a set of samples denoted with digit 3), and samples subjected to the simulated fire restricted to 600ºC during one hour followed by fast cooling with water (a set of samples denoted with number 361), no significant differences may be observed between the shapes of compared curves depicted in both Figure 14a and Figure 14b. For this scenario in both cases similar values of breaking work (230 J and 260 J) as well as longitudinal extension (2.10 mm and 2.44 mm) are obtained. Additionally, the curves characterizing this impact test exhibit a plateau in the final stage of the experiment indicating incomplete break in the specimen. The slow cooling of the sample in the furnace following the heating to the temperature of 600ºC (a set of samples denoted by the number 360) resulted in slow transition through the critical brittle zone at 475ºC, as a consequence a disadvantageous precipitation of secondary brittle phases occurred accompanied by a change in the δ ferrite precipitation form to the acicular secondary ferrite α'. This resulted in significant decrease in impact strength, with respect to the samples belonging to the group denoted as 361. This simulated fire scenario seems to exhibit the highest sensitivity to the testing temperature for the considered steel, as for the impact notch-toughness test conducted at +20ºC the averaged W_t breaking energy value at the level of 127 J has been obtained, and averaged longitudinal extension at the level of 2.04 mm. During tests conducted at –20ºC the respective values of 90 J and 1.44 mm have been obtained.

Preprints (www.preprints.org) | NOT PEER-REVIEWED | Posted: 28 May 2021 doi:10.20944/preprints202105.0705.v1

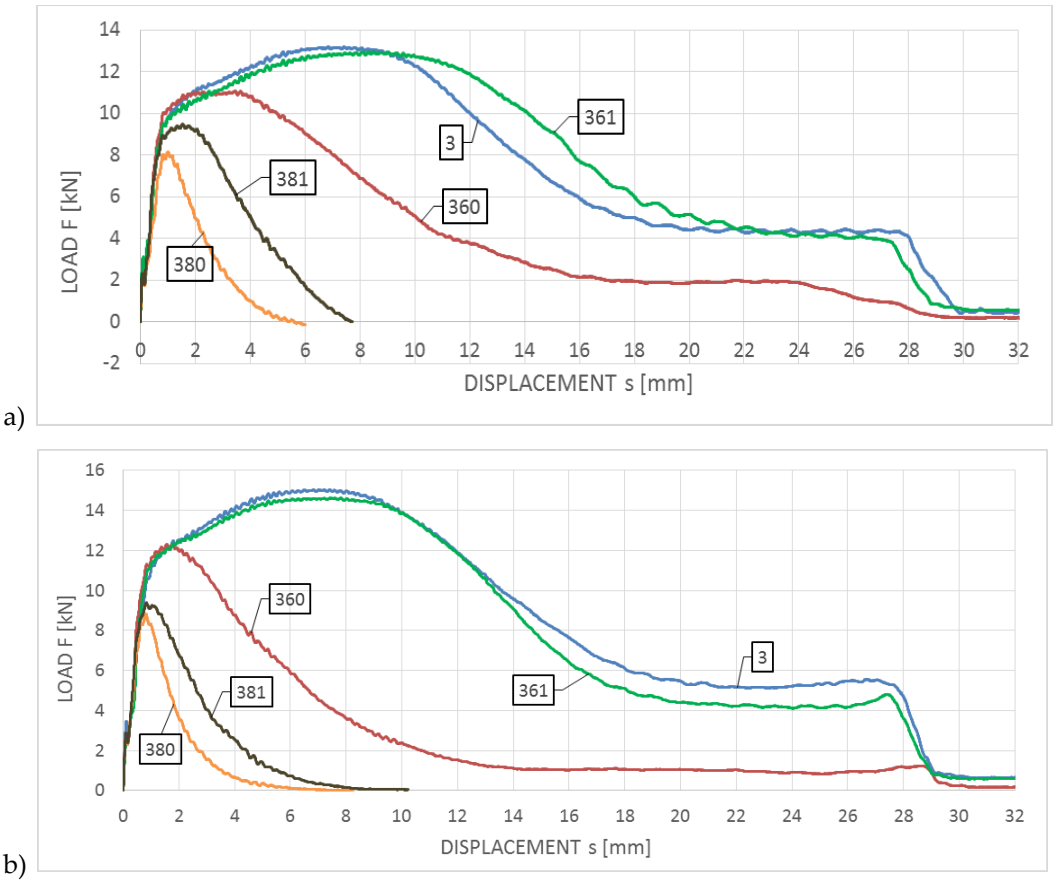

Figure 13. Averaged $F-s$ curves obtained on the samples made of X2CrNiMoN22-5-3 steel: a) during tests conducted in +20ºC, b) during tests conducted in –20ºC.

Fire scenarios related to the heating temperature of 800ºC during one hour result in intensive precipitation of numerous carbides, nitrides and intermetallic phases from supersaturated ferrite and austenite. Under such circumstances fast cooling with water (a set of samples denoted with number 381) to a certain degree neutralizes the influence of additional 475ºC brittleness. Unrestricted and slow cooling of the sample in the furnace (a set of samples denoted with number 380) results in successive occurrence of additional harmful brittle phases, thus implicating further decrease in impact strength. In this scenario, in both analyzed cases, low values of the breaking work W_t (within the range of 15÷35 J) have been obtained.

6. Concluding remarks

The results obtained in the impact notch-toughness tests conducted by us, and related to selected conditions simulating prior action of fire temperature on the analysed samples followed by two sample cooling scenarios after fire seem to indicate different behaviour of each tested steel grade when subjected to such conditions. Thus they may constitute a basis for drawing relatively reliable conclusions regarding post-fire susceptibility of a given material to the initiation and propagation of brittle cracks, and this seems to be crucial for the assessment of its suitability for further use. Of the steels covered in this research, especially the steels similar in behaviour to the S355J2+N grade seem to be remarkably prone to the destruction of this type. This statement refers in particular to the winter conditions, as under those conditions a zone of unstable crack growth manifests itself in a pronounced manner. Let us note, however, that the simulated fire scenario, which, of all considered, proved itself to affect the impact strength of steel S355J2+N in a least adverse manner, at the same time affected the impact strength of steel

Preprints (www.preprints.org) | NOT PEER-REVIEWED | Posted: 28 May 2021 doi:10.20944/preprints202105.0705.v1

1H18N9T in the most adverse manner. The X2CrNiMoN22-5-3 steel exhibited during tests very high sensitivity to the heating temperature. Its susceptibility to brittle fracture after heating to 800ºC during one hour proved to be substantially higher than the one obtained after heating to only 600ºC during the same time. At the lower heating temperature the cooling regimen substantially affects the final impact strength, as the slow cooling in the furnace results in substantial decrease in breaking work measured in experiment, especially in the simulated winter conditions.

a)

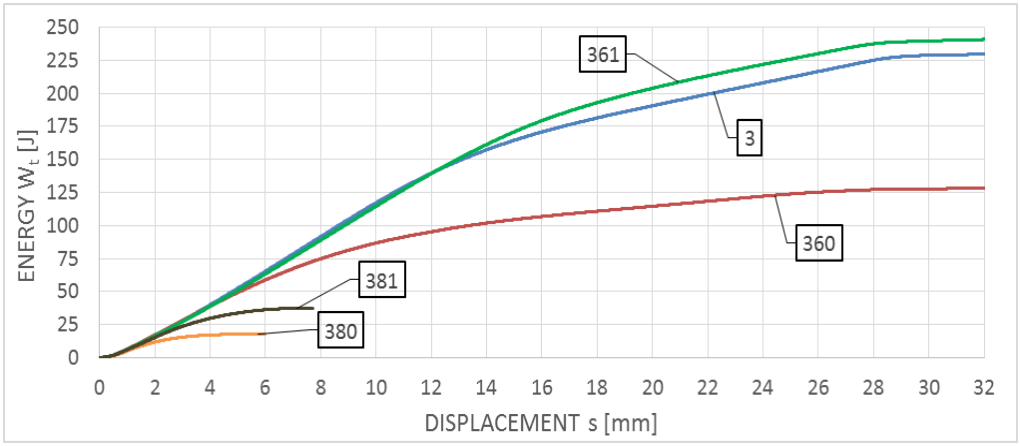

b)

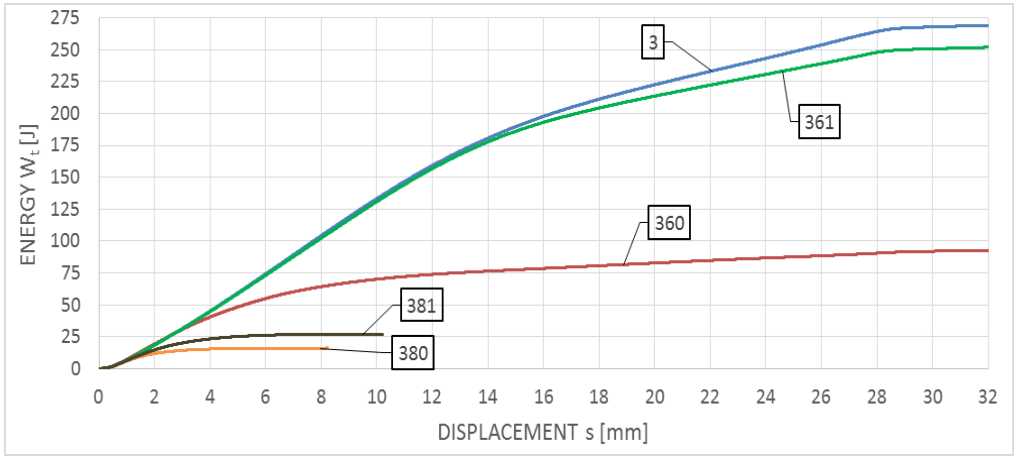

Figure 14. Averaged $W_t - s$ curves obtained on samples made of X2CrNiMoN22-5-3 steel: a) during tests conducted in +20ºC, b) during tests conducted in –20ºC.

Author Contributions: Conceptualization, M.M. and M.S.; methodology, M.S.; software, M.S. and P.Z.; validation, M.M., M.S., M.P. and P.Z.; formal analysis, M.S. and P.Z.; resources, M.S. and P.Z.; data curation, P.Z.; writing—original draft preparation, M.M., M.P. and M.S.; writing—review and editing, M.M., M.P. and M.S.; visualization, M.S and P.Z.; supervision, M.M.

Conflicts of Interest: The authors declare no conflict of interest.

References

1. Maciejewski K., Sun Y., Gregory O., Ghonem H. Time–dependent deformation of low carbon steel at elevated temperatures, *Materials Science and Engineering A*, *534*, **2012**, pp. 147-156, https://doi.org/10.1016/j.msea.2011.11.053.

2. Trilleros J.A., Mato S., Huertas I. Development of a pilot furnace for testing structural steels under standard fire model. In *Proceedings of 7th International Conference "Advances in Steel Structures" (ICASS), Nanjing, April 14-16, 2012*, Chan S.L., Shu G.P. (Eds.), vol. II, pp. 821 – 830.
3. Maslak M. Tests of structural steel after a fire in the context of assessing the possibility of its further use in the load-bearing members of building structures (in Polish), *Przegląd Budowlany*, *6*, **2012**, pp. 48-51.
4. Maslak M., Zwirski G. Changes in structural steel microstructures following heating and cooling episodes in fires, *Safety & Fire Technique*, *48*, **2017**, pp. 34-52, https://doi.org/10.12845/bitp.48.4.2017.2.
5. Bednarek Z., Kamocka R. The heating rate impact on parameters characteristic of steel behaviour under fire conditions, *Journal of Civil Engineering and Management*, *vol. XII*, *4*, **2006**, pp. 269-275, https://doi.org/10.3846/13923730.2006.9636403.
6. Peng P.C., Chi J. H., Cheng J. W. A study on behavior of steel structures subjected to fire using non-destructive testing, *Construction and Building Materials*, *128*, **2016**, pp. 170-175, https://doi.org/10.1016/j.conbuildmat.2016.07.056.
7. Müller K., Push G. Use of Charpy impact testing to evaluate crack arrest fracture toughness. In *From Charpy to present impact testing*, François D., Pineau A. (Eds.), Elsevier Science and ESIS, 2002, pp. 263-270, https://doi.org/10.1016/S1566-1369(02)80029-2.
8. Schmitt W., Varflomeyev I., Böhme W. Modelling of the Charpy test as a basis for toughness evaluation. In *From Charpy to present impact testing*, François D., Pineau A. (Eds.), Elsevier Science and ESIS, 2002, pp. 45-56, https://doi.org/10.1016/S1566-1369(02)80005-X.
9. Server W.L. Instrumented Charpy test review and application to structural integrity, In *From Charpy to present impact testing*, François D., Pineau A. (Eds.), Elsevier Science and ESIS, 2002, pp. 205-212, https://doi.org/10.1016/S1566-1369(02)80022-X.
10. Wallin K., Nevasmaa P., Planman T., Valo M. Evolution of the Charpy-V test from a quality control test to a materials evaluation tool for structural integrity assessment, In *From Charpy to present impact testing*, François D., Pineau A. (Eds.), Elsevier Science and ESIS, 2002, pp. 57-68, https://doi.org/10.1016/S1566-1369(02)80006-1.
11. Alar Ž., Mandić D., Dugorepec A., Sakoman M. Application of instrumented Charpy method in characterization of materials, *Interdisciplinary Description of Complex Systems*, *13 (3)*, **2015**, pp. 479-487, https://doi.org/10.7906/indecs.13.3.12 .
12. Zajdel P., Interpretation of the results of the impact test performed with an instrumented Charpy pendulum for the purposes of assessing the properties of structural steels (in Polish), *Inżynieria i Budownictwo*, *7*, **2020**, pp. 341 – 344.
13. Zajdel P. A suitability assessment using an instrumented impact test of the use of selected structural steel grades on the basis of their changes in response to exposure to fire, *Technical Transactions*, *vol. 118*, **2021,** https://doi.org/10.37705/techtrans-e2021007 .
14. Maslak M., Pazdanowski M., Stankiewicz M., Zajdel P. The impact strength of selected steel types after fire. Experimental tests related to simulated fire conditions. In *Proceedings of the 7th International Conference "Applications of Structural Fire Engineering" (ASFE)*, June 9-11, 2021, Ljubljana, Slovenia, Hozjan P., Pečenko R. Huč S. (Eds.).
15. Tronskar J.P., Mannan M.A., Lai M.O. Measurement of fracture initiation toughness and crack resistance in instrumented Charpy impact testing, *Engineering Fracture Mechanics*, 69, **2002**, pp. 321-338, https://doi.org/10.1016/S0013-7944(01)00077-7.
16. Canale L.C.F, Mesquita R.A., Totten G.E. *Failure analysis of heat treated steel components*, ASM International Materials Park, Ohio, USA, 2008, https://doi.org/10.31399/asm.tb.fahtsc.9781627082846 .
17. ASTM E2298-18. Standard test method for instrumented impact testing of metallic materials, https://doi.org/10.1520/E2298-18.
18. François, D. Micromechanisms and the Charpy transition curve, In *From Charpy to present impact testing*, François D., Pineau A. (Eds.), Elsevier Science and ESIS, 2002, pp. 21-31, https://doi.org/10.1016/S1566-1369(02)80003-6.
19. EN-ISO 14556, 2015, Metallic materials – Charpy V-notch pendulum impact test. Instrumented test method.
20. Curry D., Knott J.F. Effect of microstructure on cleavage fracture stress in steel, *Metal Science*, *Vol. 12*, **1978**, pp. 511-514, https://doi.org/10.1179/msc.1978.12.11.511.
21. Mengqi, Z., Shanwu, Y., Farong, W. Competition mechanism of brittle–ductile transition of metals under tensile condition, *Mechanics of Materials*, 137, **2019**, 103138, https://doi.org/10.1016/j.mechmat.2019.103138.
22. Chen L., Liu W., Yu L., Cheng Y., Ren K., Sui H., Yi X., Duan H. Probabilistic and constitutive models for ductile-to-brittle transition in steels: A competition between cleavage and ductile fracture, *Journal of the Mechanics and Physics of Solids*, *135*, **2020**, 103809, https://doi.org/10.1016/j.jmps.2019.103809.
23. Hahn G.T. The influence of microstructure on brittle fracture toughness, *Metallurgical Transactions A*, *Vol. 15A*, **1984**, pp. 947-959, https://doi.org/10.1007/BF02644685.
24. Knott J. F. The micro-mechanisms of fracture in steels used for high integrity structural components. In *Fracture, plastic flow and structural integrity. Proceedings of the 7th Symposium Organized by the Technical Advisory Group on Structural Integrity in the Nuclear Industry*, Hirsch P, Lidbury D. (Eds.), CRC Press, 2000, https://doi.org/10.1201/9780367814021-2.
25. Lin T., Evans A.G., Ritchie R.O. Stochastic modeling of the independent roles of particle size and grain size in transgranular cleavage fracture, *Metallurgical Transactions A*, *Vol. 18A*, **1987**, pp. 641-651, https://doi.org/10.1007/BF02649480.
26. Kharchenko V.V., Kondryakov E.A., Zhamaka V.N., Babutskii A.A., Babutskii A.I. The effect of temperature and loading rate on the crack initiation and propagation energy in carbon steel Charpy specimens, *Strength of Materials*, *Vol. 38*, *No. 5*, **2006**, pp. 535-541, https://doi.org/10.1007/S11223-006-0073-Y.
27. Klepaczko J.R. Impact loading on specimens of different geometries, test methods and results. In *Crack dynamics in metallic materials*, Klepaczko J.R. (Ed.), Springer – Verlag, Wien, 1990, pp. 396-398, https://doi.org/10.1007/978-3-7091-2824-4.
28. Strnadel B., Matocha K. Testing samples size effect on notch toughness of structural steels, *Metalurgija*, *48*, *4*, **2009**, pp. 253-256.
29. EN-ISO 148-1, 2006, Metallic materials – Charpy pendulum impact test. Part 1: Test method.
30. ASTM E 23-92. Standard test methods for notched bar impact testing of metallic materials, https://doi.org/10.1520/E0023-18.

31. Samuel K.G., Sreenivasan P.R., Ray S.K., Rodriguez P. Evaluating of ageing-induced embrittlement in an austenitic stainless steel by instrumented impact testing, *Journal of Nuclear Materials*, *150*, **1987**, pp. 78-84, https://doi.org/10.1016/0022-3115(87)90095-X.